

Enhanced Fabry–Perot resonance in GaAs nanowires through local field enhancement and surface passivation

Shermin Arab^{1,†}, P. Duke Anderson^{1,†}, Maoqing Yao^{1,†}, Chongwu Zhou^{1,3,†}, P. Daniel Dapkus^{1,2,3,†}, Michelle L. Povinelli^{1,†}, and Stephen B. Cronin^{1,2,†} (✉)

¹ Department of Electrical Engineering, University of Southern California, Los Angeles, CA 90089, USA

² Department of Physics, University of Southern California, Los Angeles, CA 90089, USA

³ Department of Chemical Engineering and Materials Science, University of Southern California, Los Angeles, CA 90089, USA

[†] Center for Energy Nanoscience, University of Southern California, Los Angeles, CA 90089, USA

Received: 23 January 2014

Revised: 05 April 2014

Accepted: 15 April 2014

© Tsinghua University Press
and Springer-Verlag Berlin
Heidelberg 2014

KEYWORDS

MOCVD,
GaAs,
nanowires,
photoluminescence,
Fabry-Perot,
ionic liquid

ABSTRACT

We report substantial improvements in the photoluminescence (PL) efficiency and Fabry–Perot (FP) resonance of individual GaAs nanowires through surface passivation and local field enhancement, enabling FP peaks to be observed even at room temperature. For bare GaAs nanowires, strong FP resonance peaks can be observed at 4 K, but not at room temperature. However, depositing the nanowires on gold substrates leads to substantial enhancement in the PL intensity (5X) and 3.7X to infinite enhancement of FP peaks. Finite-difference time-domain (FDTD) simulations show that the gold substrate enhances the PL spectra predominately through enhanced absorption (11X) rather than enhanced emission (1.3X), predicting a total PL enhancement of 14X in the absence of non-radiative recombination. Despite the increased intensity of the FP peaks, lower Q factors are observed due to losses associated with the underlying gold substrate. As a means of reducing the non-radiative recombination in these nanowires, the surface states in the nanowires can be passivated by either an ionic liquid (1-ethyl-3-methylimidazolium bis(trifluoromethylsulfonyl)imide (EMIM TFSI)) or an AlGaAs surface layer to achieve up to 12X enhancement of the photoluminescence intensity and observation of FP peaks at room temperature without a gold substrate.

Semiconductor nanowires with high surface-to-volume ratios possess several advantageous optoelectronic properties such as enhanced light absorption [1, 2], electrostatic gate tenability [3], and enhanced carrier

collection [4] that are beneficial for a variety of applications including detectors [5, 6], sensors [7, 8], energy storage [9], and lasers [10]. Nanowire lasers based on binary semiconductor materials are of particular

Address correspondence to scronin@usc.edu

interest because of their wide range of band gaps. GaN, GaAs, ZnO, and CdS are a few of the materials widely studied as nanolasers [11]. The first electrically pumped nanowire laser was presented by Duan et al., where the electroluminescence spectra and lasing of an *n*-type CdS nanowire were observed under an applied current of 200 μ A [12]. ZnO electroluminescence and photoluminescence (PL) were reported at room temperature by Chu et al. [13]. Fukui and coworkers reported the observation of Fabry-Perot (FP) resonances and lasing of InGaAs/GaAs core-shell nanopillars [14, 15]. One of the main challenges associated with GaAs nanowire-based optoelectronic and photonic devices is the non-radiative recombination associated with surface states, which is particularly pronounced in GaAs nanowires with high surface-to-volume ratios [16]. While many studies discuss the effects of surface passivation of bulk GaAs [17–19] and GaAs nanowires, none have investigated these effects on the FP resonance.

Here, we report a systematic study of the environmental effects on the FP resonance and photoluminescence intensity of *n*-type GaAs nanowires, including both AlGaAs-passivation and ionic liquid-passivation. The PL intensity and FP resonance quality factor are studied as a function of passivation and substrate material. PL spectra are collected at 4 K and room temperature in order to assess the carrier recombination dynamics. Finite-difference time-domain (FDTD) simulations are carried out in order to separate the effects of local field enhanced absorption from enhanced emission in the overall photoluminescence process and provide a deeper understanding of the environmental dependence of the intensities and quality factors of the PL and FP resonance.

In the work presented here, *n*-type GaAs nanowires are synthesized by metal organic chemical vapor deposition (MOCVD) with selective area growth (SAG). Trimethylgallium (TMGa), trimethylaluminum (TMAI), and arsine are used as precursors for Ga, Al, and As deposition, respectively, and disilane is used as a precursor for Si doping [20]. A thermally grown silicon oxide layer is used as a mask for the SAG growth. An array of holes (1 mm \times 1 mm) with 600 nm pitch are patterned with silicon nitride using electron beam lithography (EBL) and wet chemical etching.

Nanowires are grown in a Thomas Swan MOCVD system at a pressure of 0.1 atm. The total flow rate of the carrier gas is 7 standard liters per minute (SLM), and the partial pressure of TMGa, arsine, and disilane are 7.56×10^{-7} atm, 2.14×10^{-4} atm, and 1.43×10^{-8} atm during the growth of the nanowire core. During the growth of AlGaAs passivation layer, the arsine partial pressure was increased to 1.07×10^{-3} atm, and the partial pressures of TMGa and TMAI were kept at 3.78×10^{-7} atm and 1.51×10^{-6} atm for 120 seconds, resulting in an approximate AlGaAs thickness of 20 nm. The growth temperature was fixed at 760 $^{\circ}$ C for both the nanowire core and passivation layer. These nanowires are grown vertically along the (111)B direction, as shown in Fig. 1(a), sonicated in isopropyl alcohol, and then deposited onto various substrates including Si substrates with 300 nm of SiO₂ and Si/SiO₂ substrates with 200 nm of Au (Fig. 1(b)). Micro-Raman and photoluminescence spectroscopy were collected using a 40X objective lens, an 1,800 l/mm grating, and a silicon charged-couple device (CCD) detector to detect the PL in the range of 750 nm to 950 nm. Low to moderate power excitation (10^2 – 10^5 mW/cm²) using a 532 nm laser was used to avoid optical heating.

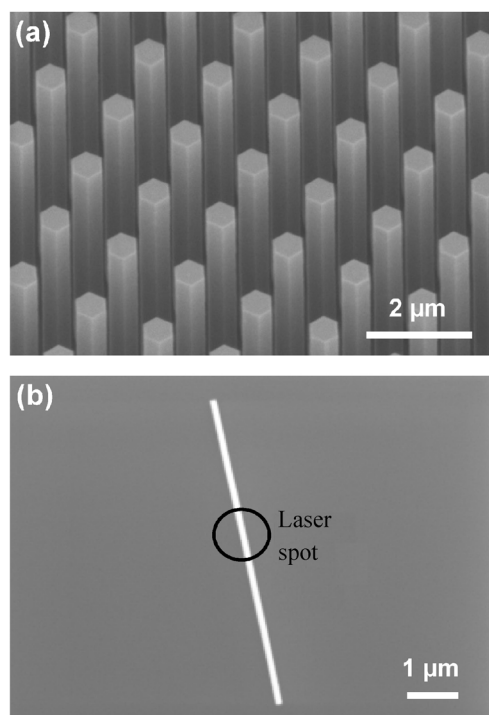


Figure 1 SEM images GaAs nanowires (a) as grown and (b) deposited on a Si/SiO₂ substrate.

Figure 2 shows the PL spectra of individual GaAs nanowires deposited on Si/SiO₂ and Au substrates. In Fig. 2(a), spectra from both substrates were taken at 4 K and exhibit strong FP peaks. The spectrum taken on the Au film is significantly enhanced with respect to that of the Si/SiO₂. The integrated areal intensity of the dominant PL peak is 5X larger for the nanowire on the Au film, whereas the relative strength of the FP peaks are also enhanced by a factor of 3.7X. Figure 2(b) shows the PL spectra of individual nanowires at room temperature. Here, the Au substrate results in strong FP resonance peaks, which are completely absent from the nanowire deposited on the Si/SiO₂ substrate. As observed in the 4 K dataset, the integrated intensity of the main PL peak increases by a factor of 5X due to the presence of the Au substrate. The increased PL intensity is attributed to the local field enhancement from the underlying Au substrate. The *Q*-factor of the FP peaks of the nanowires deposited on the Au film is 140, and 181 for nanowires on Si/SiO₂. This decrease in *Q*-factor

can be attributed to the lossy nature of the Au substrate. The mode spacing of the FP peaks can be calculated by the relation:

$$\Delta\lambda = \frac{\lambda^2}{2L \left[n - \lambda \left(\frac{dn}{d\lambda} \right) \right]}$$

where *n* is the refractive index and λ is the wavelength. We observe a mode spacing of 8–10 nm (at 4 K) for this 270 nm diameter and 7 μ m long nanowire deposited on Si/SiO₂, while a calculated mode spacing of 11.5 nm is obtained, assuming $n = 3.655$, and $dn/d\lambda = -0.822 \mu\text{m}^{-1}$. The difference between the experimental and calculated mode spacing can be attributed to the lack of precision in the optical microscope image of the nanowire length and/or the dispersive nature of the waveguide, which was not considered in the model [15]. A similar agreement was obtained for nanowires on Au substrates.

In order to understand the underlying mechanism of enhancement, FDTD simulations are carried out on a GaAs nanowire on top of both Si/SiO₂ and Au substrates, as illustrated in Figs. 3(a) and 3(b). In both systems, the dispersive nature of each material is taken into account and perfectly matched layers (PML) are imposed along the simulation boundaries. The 532 nm optical pump is simulated using a Gaussian beam (1.5 μ m in diameter) focused on the center of the GaAs nanowire. Here, we consider a GaAs nanowire 260 nm in diameter and 7.75 μ m in length. The resulting cross-sectional electric-field intensity distributions are plotted in Figs. 3(c) and 3(d), corresponding to the structures shown in Figs. 3(a) and 3(b), respectively. While these mode profiles look similar, the intensities obtained on the gold substrate (Fig. 3(d)) are more than one order of magnitude higher than those on the bare Si/SiO₂ substrate (Fig. 3(c)).

We can calculate the relative enhancement in the optical absorption of the nanowire due to the presence of the metallic substrate by integrating the electric-field intensity inside the hexagonal nanowire cross-section of each system and taking the ratio:

$$EF_{\text{ABS}} = \frac{\int |E_{\text{Au}}|^2 dA}{\int |E_{\text{SiO}_2}|^2 dA}$$

For an incident wavelength of 532 nm, the total electric

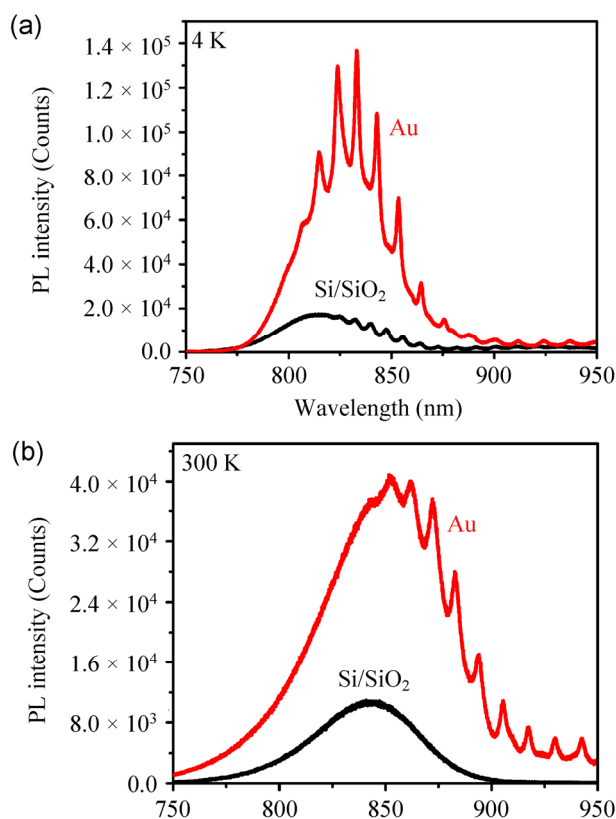


Figure 2 Photoluminescence spectra of individual GaAs nanowires taken at (a) 4 K and (b) room temperature under 532 nm excitation (3.5 μ W), deposited on Si/SiO₂ and Au substrates.

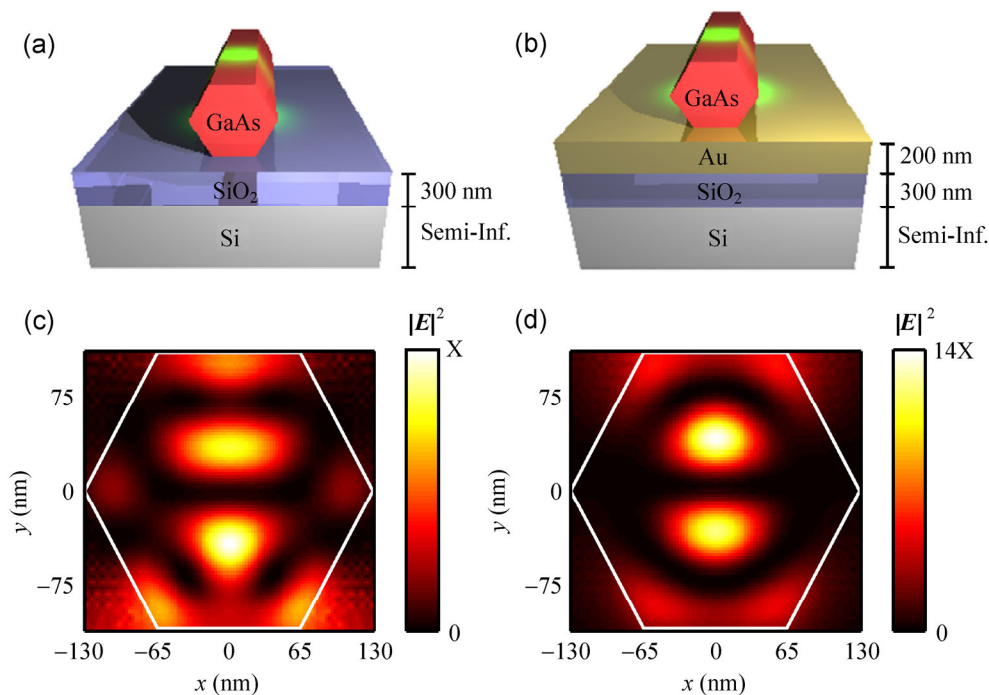


Figure 3 Schematic diagrams illustrating the two simulated pump geometries: GaAs nanowire on (a) bare Si/SiO₂ substrate and (b) 200 nm Au film on top of Si/SiO₂. The nanowire is 260 nm in diameter and 7.75 μm in length. The green spot in each diagram represents the 532 nm optical pump focused on the nanowire with a beam waist of 1.5 μm . (c) and (d) Cross-sectional electric field intensity distributions for the geometries in (a) and (b), respectively. The white outline in each plot indicates the hexagonal boundary of the nanowire. Note: The intensity scale in (d) is 14X higher than in (c).

field enhancement is 11X, indicating the gold substrate concentrates 11 times more total electric field intensity within the nanowire than the Si/SiO₂ substrate. If one considers the Au film simply as a mirror, then one would naively expect an enhancement on the order of 2X. Instead, the metal structure appears to form a cavity that traps light and results in this large enhancement factor. The mode profiles presented in Figs. 3(c) and 3(d) depend sensitively on the diameter of the nanowire, and as a result, the absorption enhancement factor (EF_{ABS}) varies significantly with nanowire diameter. A graph of the diameter dependence of the absorption enhancement is shown in the Electronic Supplementary Material (ESM). Within a diameter range of 200–300 nm, we found that a diameter around 260 nm produced the largest absorption enhancement.

PL emission is modeled in the GaAs nanowire using electric dipoles, as illustrated in Figs. 4(a) and 4(b). Each electric dipole emits at a center wavelength of 850 nm and possesses a bandwidth of 200 nm. A

Gaussian distribution is superimposed upon the emission spectra in order to resemble the PL data collected experimentally. Again, we assume our nanowire maintains a diameter of 260 nm and a length of 7.75 μm . The total dipole power (TDP) is defined as the power emitted by the dipole, calculated using a surrounding flux box (black, dashed box). The TDP is strongly affected by the local density of states, and therefore, will depend upon the dipole's position within the nanowire and its surrounding environment. The extracted power (EP) is defined as the total power collected from the top of the GaAs nanowire (black, dashed line). In order to obtain realistic spectra, nine cross-sectional dipole positions are included along with two orthogonal polarizations per position. By taking advantage of the mirror symmetry of the structure, this equates to 26 effective dipole positions. In order to avoid coherence effects, only one dipole is included per simulation. An incoherent summation is later performed on the emission results.

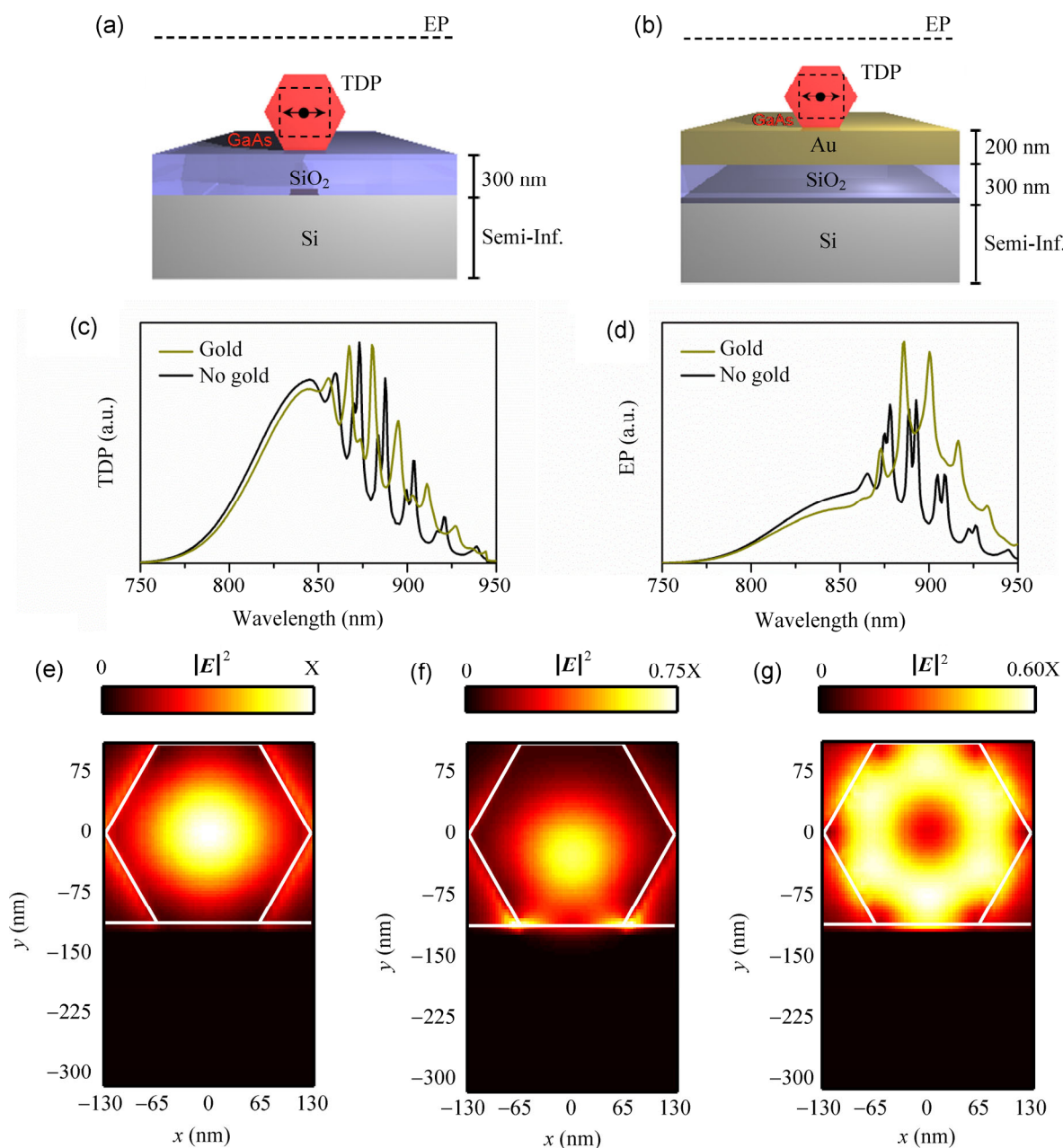


Figure 4 Schematic diagrams of the two systems simulated for PL emission: GaAs nanowire on (a) bare Si/SiO₂ substrate and (b) 200 nm Au film on top of Si/SiO₂. The dashed lines indicate flux monitors. The nanowire is 260 nm in diameter and 7.75 μm in length. Incoherent summation results for (c) the total dipole power (TDP) and (d) the extracted power (EP) of each competing topology. (e) Electric field intensity profile of the HE₁₁ FP modes of the Si/SiO₂ system. (f) Electric field intensity profile of the HE₁₁-like FP modes of the Au system. (g) Electric field intensity profile of the higher-order, TE₀₁/TM₀₁ FP mode of the Si/SiO₂ system.

Figures 4(c) and 4(d) show the TDP and EP results for both structures. FP fringes are clearly visible in the simulated spectra. The average peak-to-peak spacing and quality factors of the resonances closely resemble those found experimentally. By integrating both EP spectra and taking their ratio ($\int EP_{\text{Au}} d\lambda / \int EP_{\text{SiO}_2} d\lambda = 1.3$), we find that the gold substrate produces roughly

the same emitted power as the bare Si/SiO₂ substrate. This is somewhat surprising since one would expect the Au film to act like a mirror, reflecting light upward that would otherwise be lost to the underlying substrate. However, the losses in the Au film slightly decrease the emitted power that is collected, resulting in a combined effect near unity.

In Figs. 4(c) and 4(d), we observe two sets of peaks, particularly on the Si/SiO₂ substrate where the Q factors are higher. The dominant Si/SiO₂ substrate peak corresponds to a symmetric HE₁₁ mode, while the weaker side peak has a six-fold symmetric TE₀₁/TM₀₁ mode profile. Figures 3(e) and 3(g) show the electric field intensity profiles of each mode, respectively. Figure 3(f) shows the electric field intensity profile for the dominant peak in the Au substrate system. The electric field profile obtained on the Au film displays high intensity at the Au/GaAs interface, substantiating the losses associated with the gold film. We can quantify the absorptive power loss using the following formula:

$$P_{\text{ABS}} = \frac{1}{2} \omega |E|^2 \varepsilon''$$

where ε'' is the imaginary part of the dielectric function. By comparing the HE₁₁-like modes in each system we find that, on average, the FP modes in the gold system lead to 5.8X more power loss. This additional absorptive loss helps explain why the Q factors of these modes are lower than those associated with the Si/SiO₂ system.

Multiplying the two enhancement factors (pump absorption and extracted power), we obtain an overall photoluminescence enhancement factor of 14, where the absorption enhancement (11X) is by far the dominant effect. These enhancement factors are larger than those observed experimentally (5X). The theoretical model does not include any losses associated with non-radiative recombination which are present in the experiment.

Dangling bonds and surface states in GaAs lead to non-radiative surface recombination that is particularly pronounced in the GaAs nanowires because of their high surface to volume ratio [21–23]. This recombination lowers the photoluminescence efficiency, and results in a more lossy FP cavity. As a means of reducing the non-radiative surface recombination in these nanowires, the effect of surface passivation was explored. Here, we consider two forms of passivation: AlGaAs passivation, which leads to a core-shell structure, and ionic liquid passivation. In the former case, after the GaAs nanowire growth, a layer of AlGaAs is deposited as a passivation layer. The thickness of the AlGaAs

layer is 20 nm. The PL spectra of AlGaAs-passivated nanowires are shown in Fig. 5(a), which exhibits the FP resonance peaks at room temperature. These spectra also exhibit two sets of peaks, as in the simulation (Figs. 4(c) and 4(d)), which can be attributed to different mode symmetries. Figure 5(b) shows the PL spectra taken with and without ionic liquid passivation. Here, we deposit approximately 30 μL of the ionic liquid 1-ethyl-3-methylimidazolium bis(trifluoromethylsulfonyl)imide (EMIM TFSI) (Sigma-Aldrich) [24] to passivate the surface states in the nanowire. This form of passivation leads to a 12X enhancement in the PL intensity without applying any potential to the nanowire and enables us to observe the FP resonance at room temperature (Fig. 5(b)). Both AlGaAs-passivated and ionic liquid-passivated nanowires were measured on bare Si/SiO₂ substrates, as shown in Figs. 5(a) and 5(b). Ionic liquid passivated nanowires were also measured on Au covered substrates. While the FP

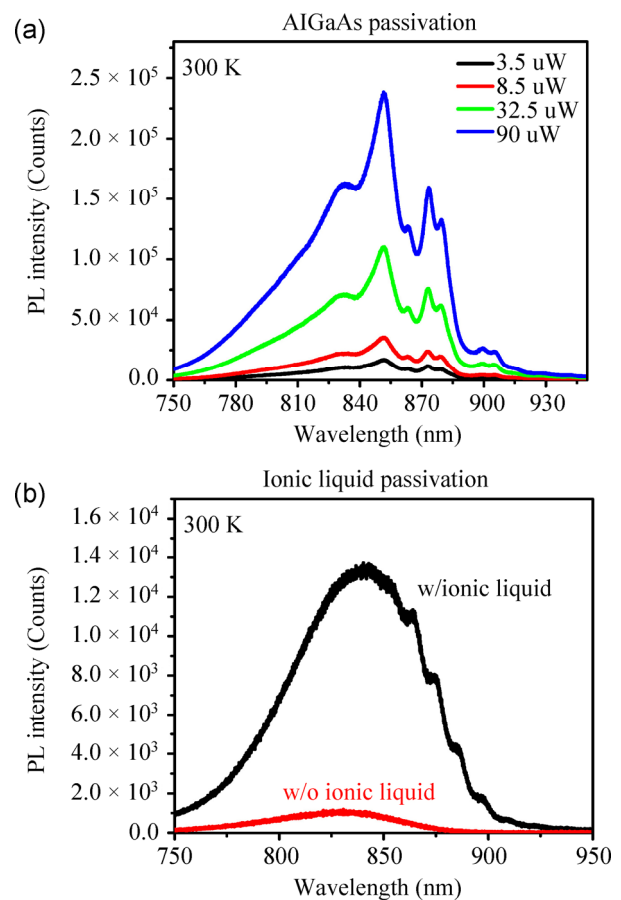


Figure 5 Room temperature PL spectra of (a) an AlGaAs-passivated nanowire and (b) an EMIM TFSI ionic liquid-passivated GaAs nanowire taken at 8.5 μW laser power intensity.

resonance peak could be observed, these peaks were quite weak compared to those obtained on the bare Si/SiO₂ substrate. It is likely that the ionic liquid is not as effective on the metal substrate due to charge screening, which weakens the ability of the ionic liquid to passivate the surface states. The PL intensity of AlGaAs passivated GaAs nanowires on Au substrates, however, results in both observation of FP peaks and an additional enhancement of 3.3X.

In conclusion, we observe enhanced photoluminescence and FP resonance in MOCVD-grown GaAs nanowires by controlling the local environment of the nanowires, either through local field enhancement or surface passivation. Depositing the nanowires on Au films leads to a PL intensity enhancement of 5X, due to increased light absorption, and finite FP peaks at room temperature. The dominant mechanism for this enhancement, as established through finite difference time domain simulations, is in the absorption of incident light rather than emission. In addition to intensity enhancement, the Q factors of the FP peaks decreases due to losses in the gold substrate. FP resonance peaks can also be observed at room temperature on bare Si/SiO₂ substrates, when passivated with either AlGaAs or ionic liquids, which enhances the PL intensity by as much as 12X. Here, the passivation of surface states reduces non-radiative surface recombination substantially, resulting in increased PL efficiency.

Acknowledgement

This material is based upon work supported as part of the Center for Energy Nanoscience (CEN), an Energy Frontier Research Center (EFRC) funded by the U.S. Department of Energy, Office of Science and Office of Basic Energy Sciences, under Award DE- SC0001013.

Electronic Supplementary Material: Supplementary material is available in the online version of this article at <http://dx.doi.org/10.1007/s12274-014-0477-0>.

References

- [1] Lin, C. X.; Povinelli, M. L. Optimal design of aperiodic, vertical silicon nanowire structures for photovoltaics. *Opt. Express* **2011**, *19*, A1148–A1154.
- [2] Madaria, A. R.; Yao, M. Q.; Chi, C. Y.; Huang, N. F.; Lin, C. X.; Li, R. J.; Povinelli, M. L.; Dapkus, P. D.; Zhou, C. W. Toward optimized light utilization in nanowire arrays using scalable nanosphere lithography and selected area growth. *Nano Lett.* **2012**, *12*, 2839–2845.
- [3] Cui, Y.; Zhong, Z. H.; Wang, D. L.; Wang, W. U.; Lieber, C. M. High performance silicon nanowire field effect transistors. *Nano Lett.* **2003**, *3*, 149–152.
- [4] Kelzenberg, M. D.; Boettcher, S. W.; Petykiewicz, J. A.; Turner-Evans, D. B.; Putnam, M. C.; Warren, E. L.; Spurgeon, J. M.; Briggs, R. M.; Lewis, N. S.; Atwater, H. A. Enhanced absorption and carrier collection in Si wire arrays for photovoltaic applications. *Nat. Mater.* **2010**, *9*, 239–244.
- [5] Liu, D. K.; You, L. X.; Chen, S. J.; Yang, X. Y.; Wang, Z.; Wang, Y. L.; Xie, X. M.; Jiang, M. H. Electrical characteristics of superconducting nanowire single photon detector. *IEEE Trans. Appl. Supercond.* **2013**, *23*, 2200804.
- [6] Schuck, C.; Pernice, W. H. P.; Tang, H. X. NbTiN superconducting nanowire detectors for visible and telecom wavelengths single photon counting on Si₃N₄ photonic circuits. *Appl. Phys. Lett.* **2013**, *102*, 051101.
- [7] Hasegawa, H. Control of surfaces and heterointerfaces of AlGaIn/GaN system for sensor devices and their on-chip integration on nanostructures. *Curr. Appl. Phys.* **2007**, *7*, 318–327.
- [8] Rosenberg, D.; Kerman, A. J.; Molnar, R. J.; Dauler, E. A. High-speed and high-efficiency superconducting nanowire single photon detector array. *Opt. Express* **2013**, *21*, 1440–1447.
- [9] Wu, H.; Xu, M.; Wang, Y. C.; Zheng, G. F. Branched Co₃O₄/Fe₂O₃ nanowires as high capacity lithium-ion battery anodes. *Nano Res.* **2013**, *6*, 167–173.
- [10] Hua, B.; Motohisa, J.; Ding, Y.; Hara, S.; Fukui, T. Characterization of Fabry-Pérot microcavity modes in GaAs nanowires fabricated by selective-area metal organic vapor phase epitaxy. *Appl. Phys. Lett.* **2007**, *91*, 131112.
- [11] Saxena, D.; Mokkapat, S.; Jagadish, C. Semiconductor nanolasers. *IEEE Photonics J.* **2012**, *4*, 582–585.
- [12] Duan, X. F.; Huang, Y.; Agarwal, R.; Lieber, C. M. Single-nanowire electrically driven lasers. *Nature* **2003**, *421*, 241–245.
- [13] Chu, S.; Wang, G. P.; Zhou, W. H.; Lin, Y. Q.; Chernyak, L.; Zhao, J. Z.; Kong, J. Y.; Li, L.; Ren, J. J.; Liu, J. L. Electrically pumped waveguide lasing from ZnO nanowires. *Nat. Nanotechnol.* **2011**, *6*, 506–510.
- [14] Hua, B.; Motohisa, J.; Kobayashi, Y.; Hara, S.; Fukui, T. Single GaAs/GaAsP coaxial core-shell nanowire lasers. *Nano Lett.* **2009**, *9*, 112–116.

- [15] Yang, L.; Motohisa, J.; Fukui, T.; Jia, L. X.; Zhang, L.; Geng, M. M.; Chen, P.; Liu, Y. L. Fabry-Pérot microcavity modes observed in the micro-photoluminescence spectra of the single nanowire with InGaAs/GaAs heterostructure. *Opt. Express* **2009**, *17*, 9337–9346.
- [16] Chang, C.-C.; Chi, C.-Y.; Yao, M. Q.; Huang, N. F.; Chen, C.-C.; Theiss, J.; Bushmaker, A. W.; LaLumondiere, S.; Yeh, T.-W.; Povinelli, M. L.; et al. Electrical and optical characterization of surface passivation in GaAs nanowires. *Nano Lett.* **2012**, *12*, 4484–4489.
- [17] Offsey, S. D.; Woodall, J. M.; Warren, A. C.; Kirchner, P. D.; Chappell, T. I.; Pettit, G. D. Unpinned (100) GaAs surfaces in air using photochemistry. *Appl. Phys. Lett.* **1986**, *48*, 475–477.
- [18] Yablonovitch, E.; Sandroff, C. J.; Bhat, R.; Gmitter, T. Nearly ideal electronic-properties of sulfide coated GaAs surfaces. *Appl. Phys. Lett.* **1987**, *51*, 439–441.
- [19] Wilmsen, C. W.; Geib, K. M.; Shin, J.; Iyer, R.; Lile, D. L.; Pouch, J. J. The sulfurized InP surface. *J. Vac. Sci. Technol. B*, **1989**, *7*, 851–853.
- [20] Yao, M. Q.; Madaria, A. R.; Chi, C. Y.; Huang, N. F.; Lin, C. X.; Povinelli, M. L.; Dapkus, P. D.; Zhou, C. W. Scalable synthesis of vertically aligned, catalyst-free gallium arsenide nanowire arrays: Towards optimized optical absorption. In *Proc. SPIE 8373, Micro- and Nanotechnology Sensors, Systems, and Applications IV*, Baltimore, Maryland, USA, 2012, pp 837314.
- [21] Sheldon, M. T.; Carissa, N. E.; Harry, A. A. GaAs passivation with trioctylphosphine sulfide for enhanced solar cell efficiency and durability. *Adv. Energy Mater.* **2012**, *2*, 339–344.
- [22] Demichel, O.; Heiss, M.; Bleuse, J.; Mariette, H.; i Morral, A. F. Impact of surfaces on the optical properties of GaAs nanowires. *Appl. Phys. Lett.* **2010**, *97*, 201907.
- [23] Perera, S.; Fickenscher, M. A.; Jackson, H. E.; Smith, L. M.; Yarrison-Rice, J. M.; Joyce, H. J.; Gao, Q.; Tan, H. H.; Jagadish, C.; Zhang, X.; Zou, J. Nearly intrinsic exciton lifetimes in single twin-free GaAs/AlGaAs core-shell nanowire heterostructures. *Appl. Phys. Lett.* **2008**, *93*, 053110.
- [24] Alarcón-Lladó, E.; Mayer, M. A.; Boudouris, B. W.; Segalman, R. A.; Miller, N.; Yamaguchi, T.; Wang, K.; Nanishi, Y.; Haller, E. E.; Ager, J. W. PN junction rectification in electrolyte gated Mg-doped InN. *Appl. Phys. Lett.* **2011**, *99*, 102106.